The Role of Conserved Histidines in the Structure and Stability of Human Papillomavirus Type 16 E2 DNA-Binding Domain†

Kakoli Bose,‡ Nicholas C. Yoder,§ Krishna Kumar,§ and James D. Baleja*,‡

Department of Biochemistry, Tufts University School of Medicine, Boston, Massachusetts 02111, and Department of Chemistry, Tufts University, Medford, Massachusetts 02155

Received June 6, 2006; Revised Manuscript Received November 20, 2006

ABSTRACT: The E2 protein of papillomavirus is the key regulator of viral transcription and replication. Dimerization, which takes place via its conserved C-terminal DNA-binding domain (DBD), is critical for these functions. The presence and conservation of two histidines (H290 and H320) at or near the dimer interface suggests the importance of their roles in protein structure and stability that was explored by mutating them to neutral alanine. The H290A mutant but not the H320A mutant showed a significant change in the secondary as well as tertiary structure, as monitored by far- and near-UV circular dichroism and fluorescence. We show that the wild-type DBD was more stable than either of the two histidine mutants at pH 7.5 but that the order of stability changed with pH, where, at pH 4.5, the H290A mutant was most stable. Although H290 is important for pH dependence of the stability, it is not critical for dimerization or folding. The determination of pK_a values for the solvent-exposed histidine residues shows that the surface properties of the protein change with pH, suggesting different interactions that can be made by the protein in response to cellular acidification. Moreover, identification of residues crucial for E2 stability will help in the design of modified proteins with desired characteristics.

Papillomavirus infection is associated with cervical cancer, which is a leading cause of death in women around the globe. Of over 100 types known thus far, human papillomavirus type 16 (HPV-16) is the most common high-risk type and alone is responsible for about 50% of cervical cancers (*1*). The E2 protein of papillomaviruses plays a central role in viral transcription and replication and therefore is a key regulator of the viral life cycle. The E2 structure and function has been studied extensively (*2*). The HPV-16 E2 protein comprises 365 amino acids with three domains (*3*): a 200 amino acid N-terminal transactivation domain (TAD)[1] separated from an 85 amino acid C-terminal DNA-binding and dimerization domain (DBD) by an 80-residue hinge region (Figure 1A). The amino acids of the TAD and DBD are conserved among the papillomaviruses, whereas those of the hinge region are not.

The crystal and solution structures of E2 DBD proteins from different human and bovine types have been solved, including HPV-16 (*4*−*7*). They have similar structures that comprise a dimer, with each subunit contributing an antiparallel four-stranded β sheet and two α helices (α_1 and α_2). Helix α_1 is the recognition helix, comprising the amino acid residues involved in specific DNA sequence interactions. Upon dimerization, the β_2 and β_4 strands at the edges of each subunit participate in a hydrogen-bonding network between the subunits, thus forming an eight-stranded β-barrel structure (Figure 1B). The dimer interface of HPV-16 E2 DBD comprises the side chains of I288, H290, W319, W321, T334, T336, and M363, which are highly conserved among different human types (Figure 1C) (*5*). These residues are not conserved in bovine papillomavirus type 1 (BPV-1), where the core is less polar, suggesting that different stabilizing forces act at the dimer interfaces.

The transcriptional regulation and replication functions of E2 are mediated through binding a palindromic DNA sequence ACCgN_4cGGT, where the ACC and CGT are required for tight binding, the lower case letters indicate preferred nucleotides, and "N_4" is the central spacer region, whose sequence preference influences the binding mechanism and specificity of different types (*8*), that is manifested by the structures for BPV-1 (*9*), HPV-18 (*10*), and HPV-16 (*11*) complexed to DNA. E2 protein binds DNA via multiple pathways that include a monomer−dimer equilibrium, with the final form being a dimer bound to DNA (*12*).

There are two conserved histidines (H290 and H320) in the E2 protein sequences from high-risk human papillomaviruses. Among the other three nonconserved histidines, H308 resides on the outer face of the recognition helix (α1) and H324 and H328 are in a flexible loop that contacts the DNA phosphodiester backbone (*5*, *6*). In the protein dimer interface, the two H290 residues reside in the hydrophobic core of the protein on the β1 strand (~5 Å distance between the midpoints of the imidazole rings), while the two H320 residues lie at the base of the β barrel (~13 Å distance between the rings) with their side chains exposed to the

† This work was supported by Grants CA97922, GM65500, and S10RR017948 from the National Institutes of Health.

* To whom correspondence should be addressed: Department of Biochemistry, Tufts University School of Medicine, 136 Harrison Ave., Boston, MA 02111. Telephone: (617) 636-6872. Fax: (617) 636-2409. E-mail: jim.baleja@tufts.edu.

‡ Tufts University School of Medicine.

§ Tufts University.

[1] Abbreviations: DBD, DNA-binding domain; DCl, deuterium chloride; DTT, dithiothreitol; EDTA, ethylenediaminetetraacetic acid; IPTG, isopropyl-β-D-1-thiogalactopyranoside; M_r, reduced molecular weight; NaOD, deuterated sodium hydroxide; PEI, polyethyleneimine; TAD, transactivation domain.

10.1021/bi0611255 CCC: $37.00
Published on Web 01/10/2007

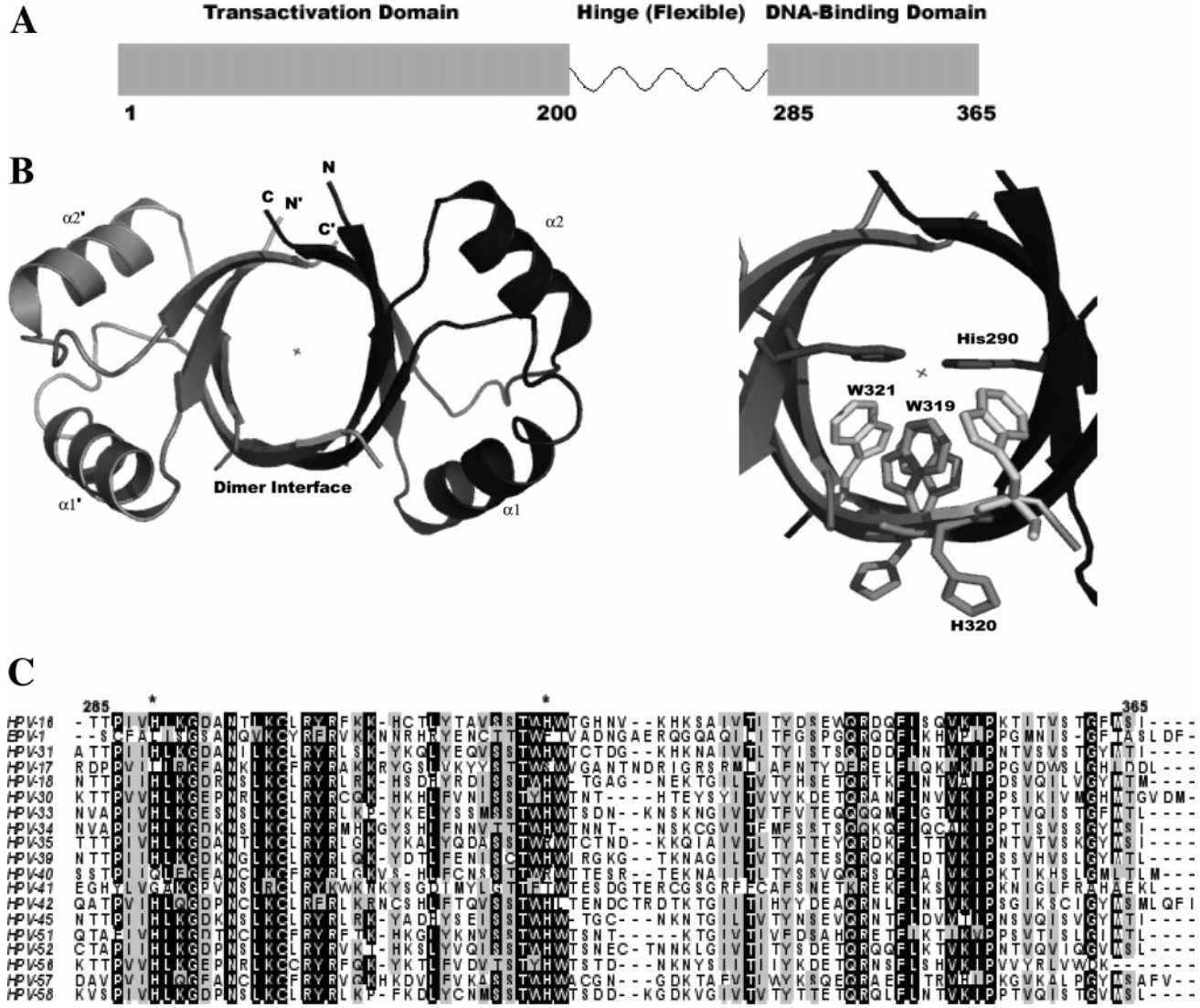

FIGURE 1: (A) Cartoon illustrating the domain structure of the HPV-16 E2 protein. (B) (Left) Structure of the HPV-16 E2 DNA-binding/dimerization domain generated from PDB entry code 1BY9. The structure comprises a central β barrel at the dimer interface and four α helices (two from one monomer, α_1 and α_2, and two from the other monomer, α_1' and α_2'). (Right) Expansion of the dimer interface. Important residues are shown labeled for only one monomer for clarity. A solvent molecule at the dimer interface is represented by "×". Distances between the midpoints of the imidazole rings are ~5 Å in the H290−H290 pair and ~13 Å in the H320−H320 pair. (C) Sequence alignment of the DNA-binding domain of E2 proteins from several high-risk types of human papillomaviruses and BPV-1 using CLUSTALW. The black shade indicates that >70% of the residues are identical, whereas the gray shade indicates >70% similarity. The two conserved histidines, H290 and H320, are indicated by asterisks.

solvent (Figure 1B). Although generally the interface of a protein includes charged residues that are neutralized by opposite charges from the same or opposite monomer (*13*), this rule does not appear to apply to the high-risk human papillomavirus E2. Here, the H290 residues face each other in a unique orientation that suggests a structural and functional significance. Lowering the pH from 8.0 to 5.5 causes a decrease in stability by ~3 kcal mol^{-1}, and the association constant (K_a) for dimer formation decreases by 2 orders of magnitude (*14*). This pH-dependent destabilization might be due to protonation of histidine residues at or near the dimer interface. To test this hypothesis, we mutated H290 and H320 to neutral alanine individually and studied their effects on the conformation and stability of the protein as a function of pH.

The HPV-16 E2 protein has excellent properties for biophysical studies. There are two buried tryptophan residues (W319 and W321) at the dimer interface in a herringbone arrangement with respect to each other (*5*) (Figure 1B) that provide an excellent tool to study the changes in the tertiary-structural environment spectroscopically by fluorescence and near-ultraviolet circular dichroism (UV CD). Also, the secondary-structural changes were monitored by far-UV CD. Equilibrium unfolding studies were used to measure the pH-dependent stability of the proteins. Oligomeric properties were determined by sedimentation equilibrium studies. The pK_a values for the titratable groups were determined by experiments that were monitored using fluorescence and nuclear magnetic resonance (NMR) as a function of pH and suggest possible roles of the histidines in acid-induced changes in the E2 protein.

Elucidation of protein conformational changes and stability is key to understanding protein function. Papillomavirus E2 protein has been a target for therapeutic intervention because

delineating a way to block function will prevent HPV replication and hence combat tumorigenesis (*15*−*18*). Understanding the dimer interface better and identifying the residues critical for its conformation and stability is important for understanding E2 function and for manipulating the dimer interface in new constructs bearing desired characteristics and is an essential step toward the development of a new class of molecules that would inhibit wild-type (WT) E2 function (*16*).

MATERIALS AND METHODS

Plasmid Construction. Construct WT, comprising residues 283−365 of HPV-16 E2 with additional Met and Val at the N terminus, was created by deleting 38 residues from the N terminus of a longer version of E2 DBD (*19*), using the Quick-change site-directed mutagenesis kit (Stratagene). The forward primer was 5′-AGGAGATATACCATGGTAAGTAACACTACAC-3′, and the reverse primer was the complement sequence. In this construct, cysteine residues C300 and C309 have been mutated to serine because the cysteine-less protein was found to be less prone to aggregation than the cysteine version. The mutations were found not to be structurally perturbing as observed by spectroscopic studies and NMR (*19*, *20*). The H290A mutant was created using a forward primer of 5′-CACTACACCCATAGTAGCTTTAAAAGGTGATGC-3′ (and the complement sequence for the reverse primer), and the H320A mutant was created using a forward primer of 5′-TGTCGTCTACATGGGCTTGGACAGGACATAATG-3′ (and the complement sequence for the reverse primer). All resulting plasmids were sequenced, and the mutations were confirmed.

Protein Purification. BL21(DE3)pLysS cells containing the plasmids were grown in Luria Bertani (LB) medium containing 25 μg/mL ampicillin and 25 μg/mL chloramphenicol at 37 °C, induced with 0.4 mM isopropyl-β-D-1-thiogalactopyranoside (IPTG) when the OD_{600} reached ∼0.6, and grown for an additional 4 h at 30 °C. Cells were harvested in a Sorvall SLA-1500, and the pellet was dissolved in 20 mL of 50 mM Tris at pH 8.0, 2 mM ethylenediaminetetraacetic acid (EDTA), and 0.1% Triton X-100 with 200 μL of protease inhibitor cocktail (Sigma). The mixture was sonicated followed by the addition of 0.5% polyethylene imine (PEI) and ammonium sulfate (30% saturation) to precipitate DNA and protein contaminants. The solution was centrifuged at 15 000 rpm for 45 min, and the supernatant was treated with 60% ammonium sulfate. The pellet was redissolved in 20 mL of 50 mM Bicine at pH 8.0, 0.5 mM EDTA, 200 mM NaCl, and 0.01% NaN_3 with 200 μL of protease inhibitor cocktail. The protein was run through an ion-exchange column (SP Sepharose Fast Flow) and eluted with a salt gradient between 200 mM and 1 M NaCl. Fractions were pooled, concentrated, and run through a gel-filtration column (Superose-12) equilibrated with 20 mM phosphate buffer at pH 6.5, 200 mM NaCl, 50 μM EDTA, and 0.01% NaN_3. The proteins obtained were greater than 95% pure as assessed by sodium dodecyl sulfate−polyacrylamide gel electrophoresis (SDS−PAGE). The concentrations were determined from the A_{280} value using the calculated extinction coefficients (*21*).

Fluorescence Emission and Far- and Near-UV CD Spectroscopy. Fluorescence emission was measured using a Fluorolog-3 spectrofluorometer (Instruments SA, Inc.). Acetate−phosphate buffer (buffer AP) was prepared by mixing 20 mM acetic acid, 200 mM NaCl, and 1 mM dithiothreitol (DTT) with 20 mM Na_2HPO_4, 200 mM NaCl, and 1 mM DTT to the desired pH. Protein (1 μM) in buffer AP was excited at 280 nm, and the emission was measured between 305 and 400 nm. The protein concentration was chosen such that the A_{280} value was below 0.1 to prevent inner-filter effects. CD was measured using a Jasco J-810 spectropolarimeter using either a 0.1 cm (far-UV) or a 1 cm (near-UV) cuvette with a 20 μM protein sample in the same buffer, except with 200 mM NaF replacing NaCl. Measurements for background correction were made by subtracting the buffer signal. Both fluorescence and CD instruments were equipped with thermostatted cell holders set to 25 °C.

Equilibrium Unfolding Studies. Protein samples (1, 2, and 5 μM) and urea stock solutions (10 M) were prepared in buffer AP as described previously (*22*). Fluorescence emission scans were acquired between 305 and 400 nm using excitation at 280 nm. CD experiments were performed by acquiring four scans at 222 nm averaged over 30 s.

The average emission wavelength $\langle\lambda\rangle$ was determined for each fluorescence spectrum using eq 1

$$\langle\lambda\rangle = \sum_{i=1}^{N}(I_i\lambda_i)/\sum_{i=1}^{N}(I_i) \quad (1)$$

where $\langle\lambda\rangle$ is the average emission wavelength and I_i is the emission at wavelength λ_i (*23*). Data were fit to the two-state model as described by eq 2

$$N_2 \xleftrightarrow{K_{eq}} 2U \quad (2)$$

where the protein is assumed to be either in its native homodimeric state (N_2) or an unfolded monomeric state (U) with their relative concentrations reflected in K_{eq}, the equilibrium constant for the transition,

$$K_{eq} = [U]^2/[N_2] \quad (3)$$

From eq 3 and the following relationship:

$$\Delta G = -RT \ln K_{eq} \quad (4)$$

where R is the gas constant and T is the temperature in Kelvin, the equilibrium constant and the ΔG are calculated with the assumption that the free-energy change is linearly dependent upon the denaturant concentration (*24*)

$$\Delta G = \Delta G_{H_2O} - m[\text{urea}] \quad (5)$$

where ΔG_{H_2O} is the free-energy change in the absence of urea and m is the cooperativity index associated with the transition. The fitting used the procedure described in ref *25* and is represented by eq 6

$$Y = (Y'_{N_2} + m'_{N_2}[\text{urea}])f_{N_2} + (Y'_U + m'_U[\text{urea}])f_U \quad (6)$$

where the amplitude of the signal, Y, is a linear combination of the fractional contribution, f, from each species, Y'_{N_2} and Y'_U are the amplitudes of the signal in the absence of urea for native and unfolded species, respectively, and m'_{N_2} and m'_U are coefficients that describe the dependence of the

signal on the concentration of urea. Six parameters, ΔG_{H_2O} (the free-energy change in the absence of urea), m (cooperativity index), Y'_{N_2}, Y'_U, m'_{N_2}, and m'_U were fitted individually for each dataset using Igor Pro (Wavemetrics, Inc.) (*25*, *26*), and the values of the free-energy change were averaged for a particular pH and protein.

Analytical Ultracentrifugation Experiments. Apparent molecular masses were determined by sedimentation equilibrium on a Beckman XL-A ultracentrifuge. Proteins were loaded at three different concentrations (4.8, 9.6, and 19.2 μM) corresponding to absorbances of 0.1, 0.2, and 0.4 at 280 nm in buffer AP with 0.5 mM DTT at pH 7.5 and 4.5. Proteins were equilibrated at rotor speeds of 16 000, 20 000, and 30 000 rpm for 18 h at 25 °C. Absorbance scans were taken at 280 and 230 nm (for the $A_{280} = 0.1$ sample) and fit to eq 7 describing homogeneous single-species sedimentation

$$\mathrm{Abs}(r) = A' \exp(HM(x^2 - x_0^2)) + E \qquad (7)$$

where Abs(r) is the absorbance at radius r, A' is the absorbance at reference radius x_0, $H = (1 - \bar{\nu}\rho)\omega^2/2RT$, with $\bar{\nu}$ being the partial specific volume of the peptide, ρ being the solvent density = 1.0069, and ω being the angular velocity in rad/s, M is the apparent molecular weight, and E is the absorbance of the blank. Data were fit using the nonlinear least-squares method implemented in Igor Pro with partial specific volumes and solution densities estimated from SEDNTERP (http://www.rasmb.bbri.org).

pH Titration by Fluorescence. Protein solutions (1 μM) in buffer AP were prepared at various pH values (9.0−3.0) and were incubated overnight at 25 °C. The average emission wavelength was determined for each dataset using eq 1, and plots of average emission wavelength versus pH were fit to eq 8 using Kaleidagraph

$$\langle\lambda\rangle = A + \Delta\langle\lambda\rangle \times 10^{n(\mathrm{pH} - \mathrm{p}K_a)}/[1 + 10^{n(\mathrm{pH} - \mathrm{p}K_a)}] \quad (8)$$

where A is the value of $\langle\lambda\rangle$ at the highest pH, $\Delta\langle\lambda\rangle$ is the change in $\langle\lambda\rangle$, n is a cooperativity parameter, and pK_a refers to the apparent pK_a value for the transition.

pH Titration by NMR. Stock protein solutions were prepared in deuterated buffer AP at pH 8.0, lyophilized, and reconstituted in 99.9% D_2O at a final protein concentration of 550 μM. Samples were left overnight at 4 °C to allow for amide exchange that would otherwise interfere with the detection of histidine Cϵ1H resonances. The pH* (direct meter reading) was adjusted between pH* 3.8 and 7.6 by adding 1 μL volumes of 100 mM deuterated sodium hydroxide (NaOD) or 100 mM deuterium chloride (DCl). One-dimensional NMR data were collected at 25 °C on a 500 MHz NMR spectrometer (Bruker AMX-500). Spectra were processed and analyzed by XWIN-NMR. A plot of chemical shifts versus pH* for each of the five histidines were fitted using nonlinear regression with Kaleidagraph (*27*), and pK_a values were obtained from the fits using the following equation:

$$\delta_{obs} = \delta_a + (\delta_{aH} - \delta_a)\{[H]^n/([H]^n + K_a^n)\} \qquad (9)$$

where δ_{obs} is the observed chemical shift at a given pH, δ_a and δ_{aH} are the calculated values for the unprotonated and the protonated forms, respectively, [H] is the proton concentration, n is the number of protons taken up or released, and K_a is the proton association constant.

Corrections were made for the deuterium isotope effect on the glass electrode and ionizable groups in the sample (*28*, *29*) by determining the pK_a of histidine in normal and deuterated buffer under otherwise identical conditions. We observed a difference of +0.3 units in D_2O, and pK_a values for the five histidines determined in D_2O were corrected to H_2O values by subtracting 0.3 units.

RESULTS

Expression and Purification of the WT and Two Histidine Mutants. This study used three constructs: the WT HPV-16 E2 sequence and two mutants. WT E2 is the DBD of E2 (residues 283−365), and the H290A and H320A mutants were obtained by site-directed mutagenesis of the WT as described under the Materials and Methods. All three proteins were analyzed by SDS−PAGE gel electrophoresis and matrix-assisted laser desorption ionization−time of flight (MALDI−TOF) mass spectrometry (Tufts University Core Facility, Boston, MA) and found to have the correct mass. The reduced monomer weight (M_r) determined for the WT was 9732 Da (calculated value of 9752 Da); M_r for H290A was 9678 Da (calculated value of 9686 Da); and M_r for H320A was 9676 Da (calculated value of 9686 Da), which agree within instrumental error.

Secondary and Tertiary Structural Properties Change Significantly upon H290A Mutation. Far-UV CD was used to assess the overall secondary-structural arrangement of the WT and two mutant proteins. The proteins showed two minima at 210 and 224 nm and a peak at ~195 nm (Figure 2A). The shift in the minima toward a longer wavelength by 2 nm from typical α-helical values was attributed to the presence of high β-sheet content (*14*). The CD spectra of the WT and H320A were superimposable, suggesting no significant secondary-structural change occurred upon the H320A mutation, whereas the H290A mutation showed a higher negative ellipticity at 224 nm. This change might be due to a rearrangement of the β-barrel core.

Near-UV CD was used to provide a measure of tertiary structure in the protein because it represents the contributions of aromatic residues as a result of their interactions with neighboring groups, and fluorescence emission was used to measure the tryptophan environment at the buried E2 interface. In near-UV CD, all three proteins showed maximum ellipticities near 277 nm (Figure 2B), suggesting predominant contributions from buried tryptophan residues. The WT and H320A gave similar spectra, while H290A showed less ellipticity and a 2 nm shift in the emission maximum toward a longer wavelength, suggesting a change in the environment of the buried tryptophan at the dimer interface. Fluorescence emission spectra of the WT and H320A (Figure 2C) showed emission maxima (335.5 and 337 nm, respectively) typical of a folded protein (*30*). The slight red shift in the wavelength maximum for H320A might be due to the mutation of a charged histidine to a neutral alanine that alters interactions with neighboring residues. In contrast, the H290A mutant showed a longer emission maximum of 343 nm, suggesting a more open and solvent-accessible dimer interface. Relative to the WT, significant quenching (~50%) was observed for the H290A mutant,

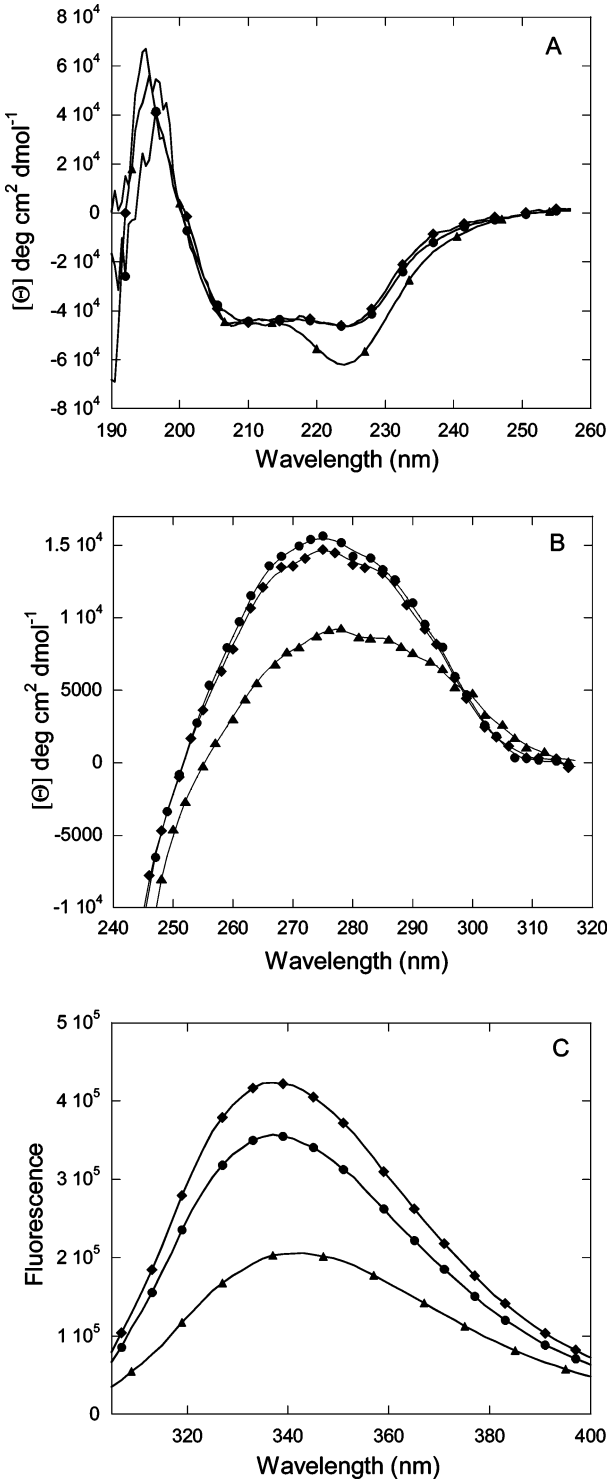

FIGURE 2: Comparison of the CD and fluorescence spectra of the WT and two mutants. (A) Far-UV CD spectra of the WT (●), H290A (▲), and H320A (◆). Experiments were performed on 20 μM samples at pH 7.5 and 25 °C. (B) Near-UV CD spectra of the WT (●), H290A (▲), and H320A (◆). Experiments were performed under the same conditions as described in A. (C) Fluorescence emission spectra of the WT (●), H290A (▲), and H320A (◆). Proteins (2 μM) were at pH 7.5 and 25 °C, and samples were excited at 280 nm.

while an increase in intensity (~20%) was observed in H320A, indicating a change in the quantum yield of the tryptophan residues. Overall, the CD and fluorescence data suggest significant secondary- and tertiary-structural changes of the protein upon H290A mutation but not the H320A mutation. These observations are supported by $^1H-^{15}N$ heteronuclear single-quantum coherence (HSQC) spectra of the three proteins (see Figure 1S in the Supporting Information). All three proteins show well-dispersed peaks, indicating that they are well-folded. For example, the NH_2 peaks at 6.5 ppm of Q345, which are shifted because of the interaction with the aromatic ring of W341, remain unchanged in all proteins. The H320A spectrum looks very similar to the WT. On the other hand, the spectrum of H290A is more different while still remaining folded. For example, the peaks at 9.6 and 9.9 ppm from residues W319 and S316 appear to have shifted to 9.3 and 9.6 ppm, respectively. Some peaks in H290A are less well-resolved and are weaker in intensity, suggesting more mobility than the WT, consistent with our other spectroscopic data.

Equilibrium Unfolding and Concentration Dependence of the WT and Mutants. The equilibrium unfolding in urea of the WT and mutants was examined to determine the effect of the mutation on conformational stability. Traces are shown in Figure 3A for the proteins at pH 7.5. We monitored changes in the secondary structure by CD and in the tertiary structure by fluorescence as a function of pH. The unfolding of the proteins was found to be reversible at all pH values as shown by the representative trace for the WT in Figure 3B. With a lowering of pH, all three proteins showed a decrease in stability and a gradual disappearance of the pretransition baseline. The data could be fit with a model in which the native dimer unfolds into a monomeric unfolded state with a single transition as described by eq 2. A plot of ΔG_{H_2O} versus pH is shown in Figure 3B, and the thermodynamic parameters are shown in Table 1. The data show that the WT is the most stable protein at pH 7.5 with $\Delta G_{H_2O} = 13.3 \pm 0.5$ kcal mol^{-1}. The stability of the WT decreases to 9.0 ± 0.2 kcal mol^{-1} at pH 4.5, whereas, for the H290A mutant, the stability changes from 12.5 ± 0.03 to 10.7 ± 0.2 kcal mol^{-1} within the same pH range. Although less stable than the WT at pH 7.5, H290A is more stable at pH 4.5 by 1.7 kcal mol^{-1}. The data demonstrate that H290 is responsible for acid-induced destabilization. Thus, reversal of stability occurs within the pH range of the histidine titration (between pH 6.0 and 4.0).

On the contrary, H320A was marginally less stable than the WT (within experimental error) at pH 7.5 and it continued to be less stable until its stability was comparable to the WT at pH 4.5 (Figure 3C). These data demonstrate that, while the conserved H320 residue is important for overall protein stability, it is not the primary determinant of pH-induced destabilization of the WT.

Experiments were done at different protein concentrations (1, 2, and 5 μM) to study concentration dependence upon equilibrium unfolding. The data were concentration-dependent over the entire pH range, indicating that the native proteins were oligomeric at all pH values (for example, for the WT at pH 7.5, $U_{50\%}$ values were 3.4 M at 5 μM and 2.9 M at 2 μM).

Oligomerization Properties as a Function of pH. To confirm that both the WT ($M_r = 9752.1$) and H290A mutant ($M_r = 9686.1$) were dimers over the pH range of 7.5 and 4.5, we used sedimentation equilibrium to determine their oligomeric states. The proteins were examined over three protein concentrations and at three rotor speeds (see the Materials and Methods). Representative data are shown in

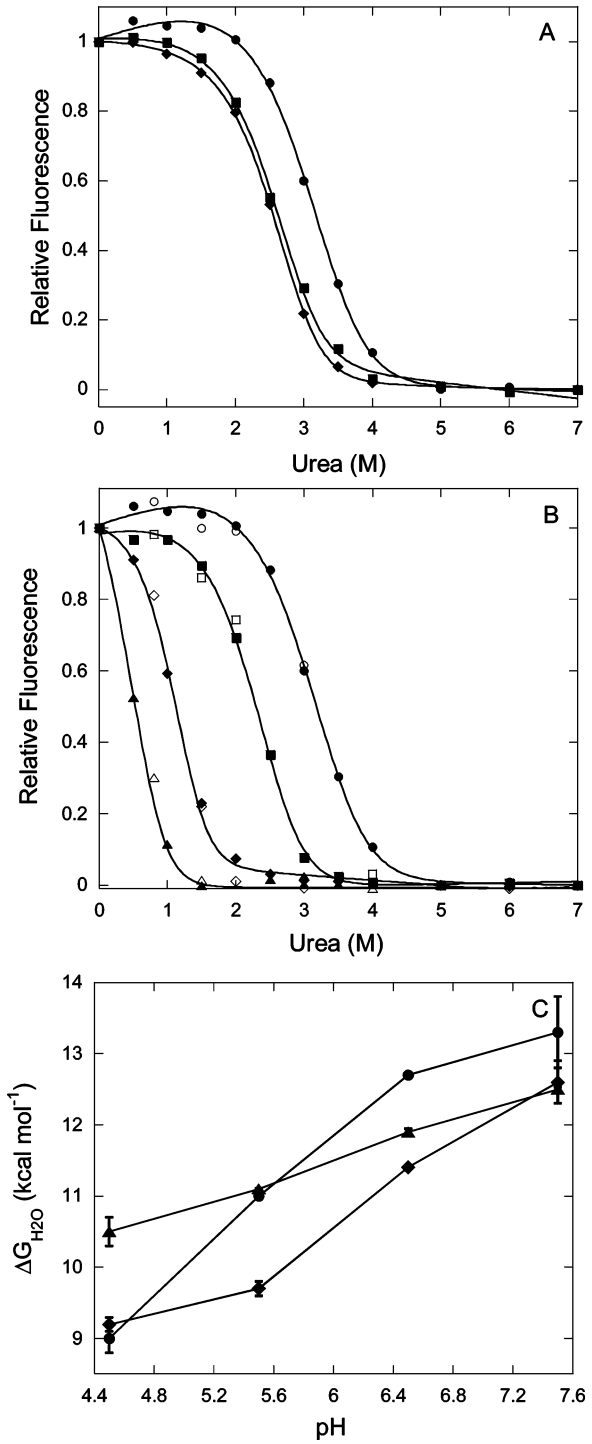

FIGURE 3: Equilibrium unfolding of the WT and two mutants. (A) Representative equilibrium unfolding data for the WT (●), H320A (■), and H290A (◆) at pH 7.5. (B) Representative equilibrium unfolding data (for the WT) at pH 7.5 (●), pH 6.5 (■), pH 5.5 (◆), and pH 4.5 (▲). Refolding data are shown as open symbols. Data for A and B were measured by recording the fluorescence average emission wavelength, with excitation at 280 nm, as a function of the urea concentration. The protein concentration was 2 μM. Solid lines represent fits to the data as described in the text, and the resultant ΔG_{H_2O}, and m values are shown in Table 1. (C) Plot of ΔG_{H_2O} versus pH for the WT (●), H290A (▲), and H320A (◆). Standard errors are indicated by vertical lines.

parts A (WT at pH 7.5), B (H290A at pH 7.5), C (WT at pH 4.5), and D (H290A at pH 4.5) of Figure 4. The data were best-fit to a single thermodynamically ideal species that corresponds to a dimer. The residuals to the fits for both proteins (parts A−D of Figure 4) demonstrate that the data are well-fit to the model. The average molecular weights were 21 454 ± 1040 and 21 212 ± 1065, respectively, for the WT and H290A at pH 7.5 and 18 920 ± 520 and 18 985 ± 613, respectively, for the WT and H290A at pH 4.5. The decreases in observed molecular weights in the WT and H290A at acidic pH are small but statistically significant. While it is tempting to attribute this to the presence of a higher percentage of the monomeric form at lower pH, we did not observe a correlation between the protein concentration and observed molecular weight; therefore, we are reluctant to make this conclusion. On the basis of its structural and folding properties, we predict that H320A has oligomeric properties similar to the WT and H290A.

Table 1: Thermodynamic Parameters of Unfolding for the WT and Mutants at Different pH Values

pH	protein	ΔG_{H_2O} (kcal mol^{-1})	m (kcal mol^{-1} M^{-1})
7.5	WT	13.3 ± 0.5	1.9 ± 0.1
	H320A	12.6 ± 0.3	2.1 ± 0.1
	H290A	12.5 ± 0.03	2.2 ± 0.1
6.5	WT	12.7 ± 0.01	2.2 ± 0.1
	H320A	11.4 ± 0.02	2.3 ± 0.01
	H290A	11.9 ± 0.05	2.4 ± 0.01
5.5	WT	11.0 ± 0.05	3.1 ± 0.01
	H320A	9.7 ± 0.1	2.4 ± 0.02
	H290A	11.1 ± 0.01	2.4 ± 0.01
4.5	WT	9.0 ± 0.2	3.1 ± 0.1
	H320A	9.1 ± 0.1	2.0 ± 0.1
	H290A	10.7 ± 0.2	2.3 ± 0.05

Identification of Titrating Groups during Acidification of E2. The change in tryptophan fluorescence with pH was studied to determine the global pK_a of the titrating groups in each protein. Because both of the buried tryptophans (W319 and W321) reside at the dimer interface, changes in fluorescence predominantly reflect changes in the environment at the interface. A third, nonconserved tryptophan (W341) is solvent-exposed on the surface on the protein and is unlikely to participate in the conformational change at the hydrophobic core of the protein. Figure 5 represents the plot of the average emission wavelength versus pH (9.0−3.4) for the WT, H320A, and H290A proteins. The WT showed a single transition between pH 6.5 and 4.5 with a pK_a of 5.0 ± 0.04. Although the titrating group is not identified here, the pK_a value suggests a histidine, an aspartate, or a glutamate residue. In H320A, the transition was still observed (although the pK_a shifted to 5.5 ± 0.04). The shift in pK_a might be the result of a subtle conformational change of the tryptophan environment at the dimer interface because of the mutation of charged histidine to neutral alanine. This conformational change is consistent with the observed red shift in the average fluorescence emission wavelength value ($\langle\lambda\rangle$ values were ∼347 nm in H320A and ∼346 nm in the WT between pH 7.0 and 9.0). In contrast, no significant transition was observed with pH for the H290A mutant, suggesting that H290 is important for the dependence on pH. These results are consistent with the far-UV CD experiments that showed that H290A underwent no significant change in CD between pH 7.5 and 4.5 in contrast to the WT (see Figure 2S in the Supporting Information).

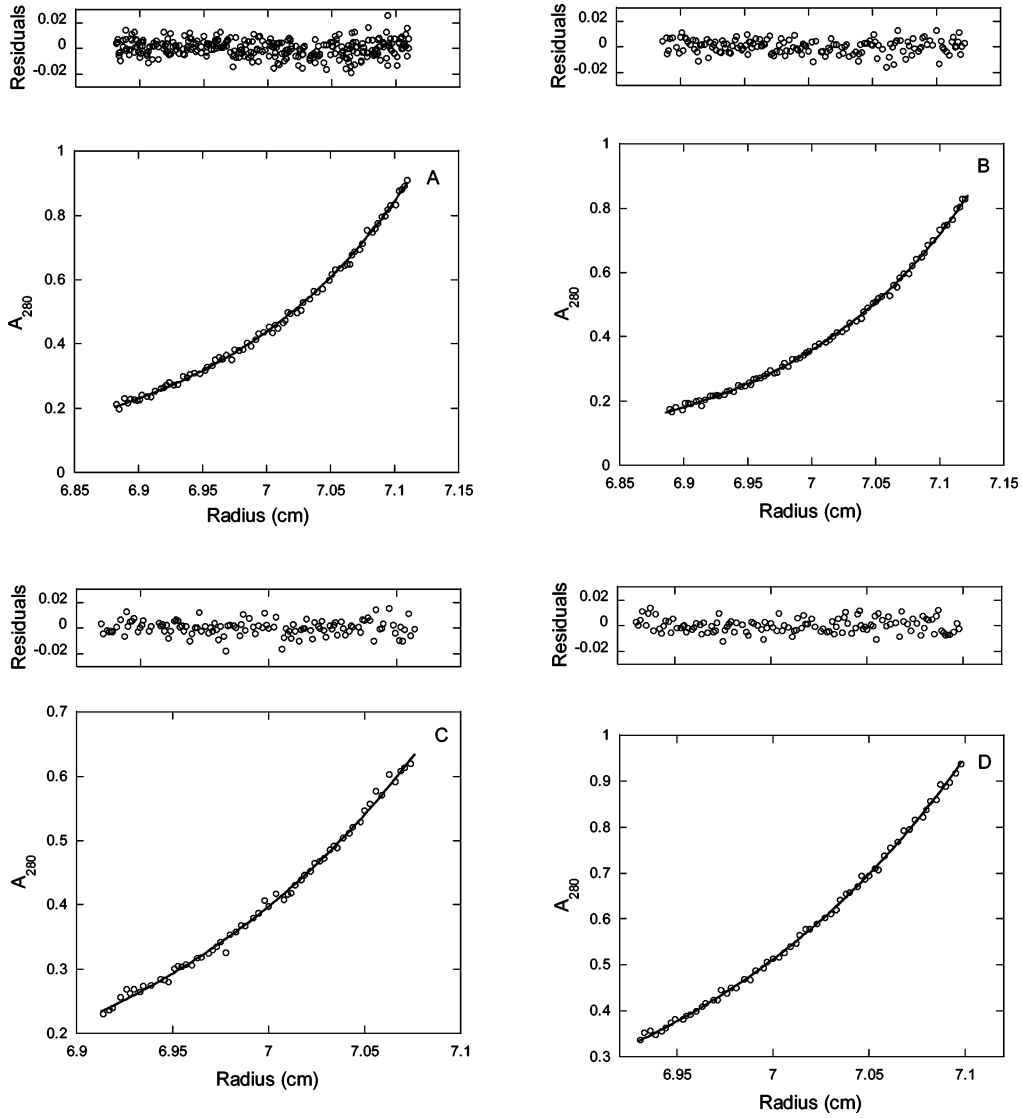

FIGURE 4: Sedimentation equilibrium studies of the WT and H290A at pH 7.5 and 4.5. The experiments were performed at 25 °C, using three rotor speeds (16 000, 20 000, and 30 000 rpm) and three different protein concentrations (corresponding to $A_{280} = 0.1$, 0.2, and 0.4). Representative traces for the WT and H290A at a concentration corresponding to $A_{280} = 0.4$ and at a rotor speed of 20 000 rpm are shown. The open circles represent the experimental data for the WT at pH 7.5 (A), H290A at pH 7.5 (B), WT at pH 4.5 (C), and H290A at pH 4.5 (D). The solid lines are the fits to the data. Residuals to the fits are shown in the panels above the corresponding data.

In addition, H290A showed the largest red-shifted average emission wavelength value of 349.5 nm of the three proteins at higher pH values (between pH 7.0 and 9.0). These observations suggest that the H290A mutation results in a more open and solvent-accessible dimer interface, whose conformation does not change with pH.

To identify some of the surface features of E2 that change upon acidification, we measured pK_a values of the histidine residues. In the NMR spectrum of the sample in D_2O, five peaks were observed for the Cϵ1H of the five histidines. Peaks for H290 (most high field) and H320 (most low field) were identified by comparing the spectrum of the WT with those of the mutants at pH 6.5, where the spectra were well-resolved (Figure 6A). Minor differences in the signal-to-noise ratio in the three spectra were not consistent at all pH values and might be due to either intrinsic differences in the line width at pH 6.5 or a variation in adjusting the homogeneity for each sample.

The chemical shifts (δ) were determined across the pH* (direct meter reading) range of 3.8−7.6 (Figure 6B) and were consistent with the published assignments at high pH (*6*). The pK_a values corrected to H_2O solution were 6.2 ± 0.03, 6.0 ± 0.02, 5.8 ± 0.02, 5.5 ± 0.02, and 4.9 ± 0.02, respectively, for the peaks from high to low field. The unusually low pK_a value of 4.9 ± 0.02 for H290 is suggestive of a buried or positively charged environment that is consistent with the solution and crystal structures of the protein. The pK_a of H290 observed by NMR was consistent with the pK_a obtained for the protein as a whole from fluorescence studies. Thus, this experiment provides evidence that H290 is the major titrating group at pH 5.0. The remaining histidines, including H320, have higher pK_a values of 5.5−6.2 and thus do not significantly contribute to the titrating group observed by fluorescence.

DISCUSSION

The imidazole ring of histidine is unique among amino acid residues. While its ionization properties change within the range of physiological pH, as a heteroatomic moiety, histidine can also interact with other aromatic and nonpolar

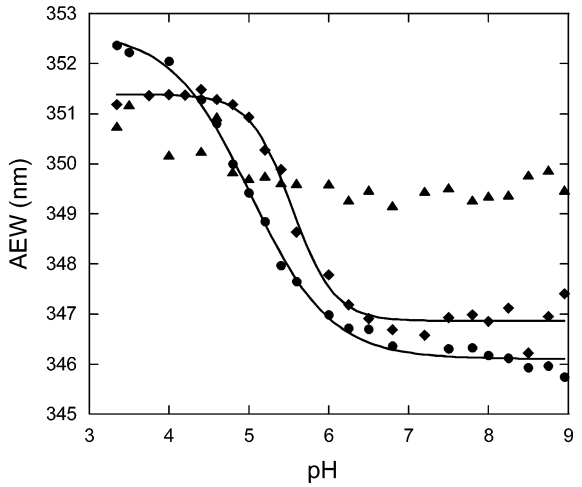

FIGURE 5: pH titration of the WT (●), H290A (▲), and H320A (◆) as monitored by fluorescence. Samples were excited at 280 nm, and the emissions were measured between 305 and 400 nm. The average emission wavelengths were plotted versus pH, and the pK_a values for the WT and H320A were obtained by fitting the data (—) as described in the text. The experiments were performed at 25 °C with 2 μM protein.

groups, while its polar atoms can be involved in hydrogen bonding. Dependent upon its protonation state, it can also form salt bridges with acidic groups. In most proteins, a His−His pair is stabilized by interactions with other chemical groups in the local environment (*31*). The crystal structure of HPV-16 E2 shows that the only stabilizing interaction of the pair of opposing H290 residues from each monomer is a hydrogen bond with a water molecule (*5*). HPV-16 E2 has another histidine residue (H320) that is conserved in different human types. Our hypothesis is that these histidines play important roles in the structure and function of E2.

Mutating H290 removes the acid-induced destabilization and changes the conformation of the protein significantly, and mutating H320 alters the stability, thus supporting the hypothesis. Far-UV CD experiments demonstrated that the H290A mutation resulted in a secondary-structural change in the protein. This result is consistent with the near-UV CD and fluorescence emission experiments that show a change in the tertiary contacts. The secondary-structural change as well as the red shift in the fluorescence emission maxima (by 7.5 nm) might be due to rearrangement of the β-barrel structure at the dimer interface as a result of the substitution of a partially charged and polar histidine residue with a neutral alanine. This possibly disrupts the interaction of the imidazole nitrogen atoms with the solvent molecule as well as changes the microenvironment of the hydrophobic core, which subsequently results in a more open conformation at the dimer interface. On the other hand, the imidazole ring in H320 faces the solvent and therefore would be expected to be less sensitive to mutation. This is evident from minimal secondary- and tertiary-structural changes in the H320A mutant as monitored by CD and fluorescence spectroscopy. The H320A mutation did lead to a slight red shift in the fluorescence emission maximum (by 1.5 nm), most likely because H320 is within hydrogen-bonding distance with S317 of the other monomer, and its mutation might cause some loss of tertiary contacts.

The global conformation and stability of the proteins were compared at different pH values. Equilibrium unfolding

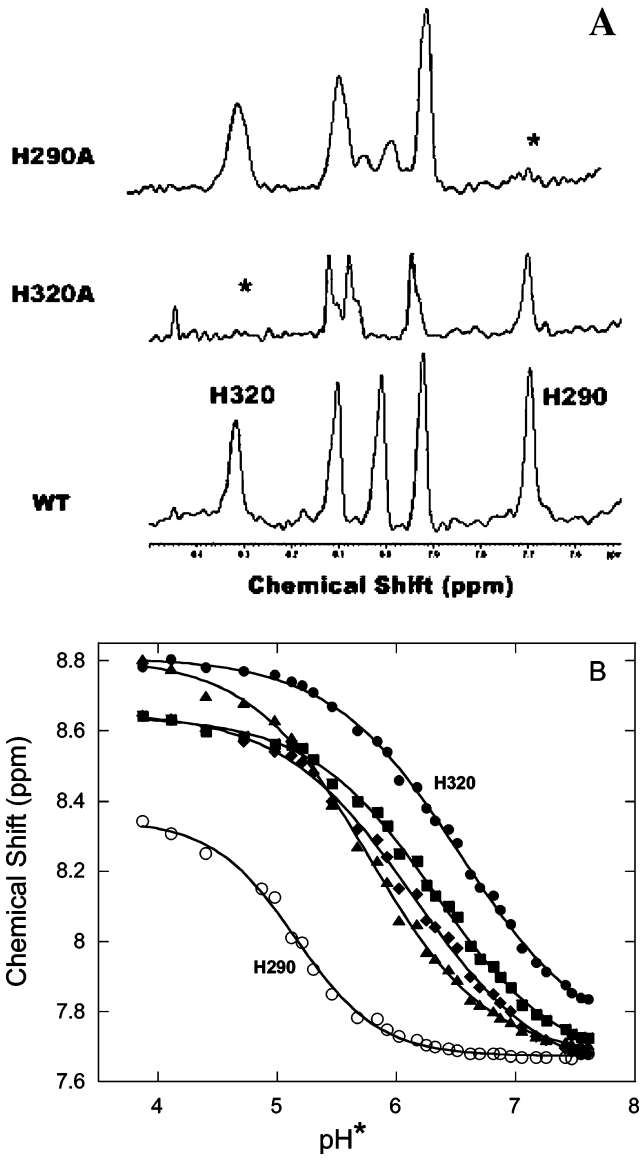

FIGURE 6: Determination of the pK_a values for individual histidine residues. (A) One-dimensional NMR spectra of the WT, H320A, and H290A showing the Cϵ1H protons of the histidines at 25 °C and pH 6.5 in D_2O. Asterisks denote missing peaks for the mutant proteins, and the assigned peaks are labeled for H290 and H320. No attempt was made to assign the other histidine residues. The presence of small shoulders in the peaks for H320A might be due to experimental variations because they were not reproducible. (B) Plot of chemical shifts (δ) versus pH for the five histidines of the WT. H290 and H320 are denoted by ○ and ●, respectively. The data were fit to the equation as described in the text (—), and the pK_a values are reported in the text.

studies showed that the stability of the proteins at pH 7.5 were in the order WT ≥ H320A ∼ H290A. The H290A and H320A mutants are likely to be less stable than the WT because of the loss of hydrogen bonding with the solvent molecule and S317, respectively. Interestingly, the order of stability was changed at pH 4.5, where H290A had the maximum stability, suggesting that H290 is primarily responsible for the acid-induced destabilization. The H290A mutant also undergoes a stability loss with pH (−1.1 kcal mol^{-1}), although less than the WT and H320A (−4.3 and −3.5 kcal mol^{-1}, respectively). Even without the histidine in H290A, the remaining pH-dependent stability depends upon contributions from different interactions most likely

because of the weakening of interactions between residues at acidic pH as well as an increase in interatomic distances (*32*). Therefore, the protonation of H290 contributes ~3.2 ± 0.5 kcal mol^{-1} to the destabilization of the E2 protein between pH 7.5 and 4.5. Consistent with these results, we find that there is very little change in the secondary and tertiary structures of H290A with pH, unlike that of the WT. Monitoring the pH titration by one-dimensional NMR identified the residue as H290. An unusually low pK_a is observed (~5.0) for H290 that is characteristic of a buried residue. Interestingly, we observed broadening of the Cϵ1H peak of H290 below pH 5.0, suggesting mobility at the dimer interface on the millisecond time scale. We also observed some unexplained chemical-shift changes upon mutation for one of the unassigned histidines with a chemical shift of 8.02 ppm at pH* 6.5 (Figure 5A). In the H320A mutant, the peak of this histidine moves downfield to 8.07 ppm, whereas in the H290A mutant, the peak appears to split into two, suggesting that this histidine is spatially close to both H320 and H290 or sensitive to mutations at these positions. H324 and H328 are the most likely candidates (on the basis of their proximity to H320, ~13 and 7 Å, respectively) and based on their positions on the flexible $\beta_2-\beta_3$ loop adjacent to the dimer interface that is affected by mutation of H290. (H308 is a poor candidate because it is >20 Å from both H320 and H290 and away from the dimer interface.) The proteins retained their dimeric states at pH 4.5 as observed by analytical ultracentrifugation experiments and retained a well-formed secondary structure at all pH values as observed using far-UV CD. This suggests that the red shift in their emission maxima upon the decrease in pH is not due to complete unfolding of the protein but rather a different protein conformation that results in an increase in solvent exposure of the interface.

Histidine-induced destabilization of the dimer interface is not unprecedented in viral proteins. For example, the trimeric envelope glycoprotein E of flavivirus requires a pH-induced reorientation of the three domains for membrane fusion. H146 from domain I and H323 from domain III undergo protonation at low pH, resulting in the disruption of hydrogen bonding across the interface between domains I and III and facilitating domain rearrangement (*33*). Histidine has also been found to play a critical role in the determination of the pH-dependent stability of the β-barrel cavity of retinol-binding protein (RBP), which is an important determinant for retinol binding and release from the enzyme (*32*). The hypothesis is that the presence of conserved histidines at the dimer interface of E2 makes it vulnerable toward acid-induced destabilization that is functionally important. H290 is conserved in human papillomaviruses, mainly in high-risk types (HPV-16, HPV-18, and HPV-31), but its specific role is unknown. The pairing of histidine residues at the dimer interface of HPV-16 E2 may act as a pH-dependent switch, and therefore, its identification is a step toward delineating the biological significance, for example, for the role of E2 in apoptosis (*34*). One possibility is that when the pH drops to ~6.8 because of cellular stress during apoptosis, the monomer−dimer equilibrium is shifted toward monomer formation (a decrease in K_{eq} by a factor of ~2.5). When we look at the equilibrium at pH 7.5 and 6.5 quantitatively and use an estimated cellular concentration of E2 of 1 nM, the lowering of pH decreases the population of dimeric E2 from 0.68 to 0.06 nM. Assuming that the in vitro situation accurately reflects conditions in the cell, the E2 protein may therefore switch from an active dimeric protein to an inactive monomeric protein under acidic conditions. Another hypothesis is that the presence of histidines at the interface leads to subtle conformational changes in the protein and changes in the surface charges that alter recognition or enhanced binding by a protein of the apoptotic machinery.

Although the precise knowledge of the physiological significance of HPV-16 E2 acidification requires further analysis, studying the dimer interface and identifying the residues crucial for conformational stability is nevertheless important because this information can aid in engineering an improved inhibitor for antiviral therapy (*16*). E2 variants lacking the N-terminal transactivation domain have been observed that repress E2 function by heterodimer formation. These truncated mutants presumably have the same dimerization capabilities as the full-length protein because they contain the same dimerization residues in the C-terminal domain. With these new data in hand, we have a basis to design an enhanced heterodimeric repressor.

ACKNOWLEDGMENT

We thank Dr. Elliot J. Androphy for review of the manuscript. We also thank Dr. Jim Sudmeier for helpful suggestions on the NMR titration experiments and Joseph Dineen for help with preparation of samples.

SUPPORTING INFORMATION AVAILABLE

Figure 1S, representing HSQC spectra of the WT and H320A and H290A mutants, and Figure 2S, showing pH-dependent secondary-structural changes of the WT and H290A mutant. This material is available free of charge via the Internet at http://pubs.acs.org.

REFERENCES

1. zur Hausen, H. (1996) Papillomavirus infections—A major cause of human cancers, *Biochim. Biophys. Acta 1288*, F55−F78.
2. Hegde, R. S. (2002) The papillomavirus E2 proteins: Structure, function, and biology, *Annu. Rev. Biophys. Biomol. Struct. 31*, 343−360.
3. Giri, I., and Yaniv, M. (1988) Structural and mutational analysis of E2 trans-activating proteins of papillomaviruses reveals three distinct functional domains, *EMBO J. 7*, 2823−2829.
4. Hegde, R. (1995) Structure of the BPV-1 E2 DNA-binding domain bound to its DNA target, *J. Nucl. Med. 36* (supplement), 25S−27S.
5. Hegde, R., and Androphy, E. (1998) Crystal structure of the E2 DNA-binding domain from human papillomavirus type 16: Implications for its DNA binding-site selection mechanism, *J. Mol. Biol. 284*, 1479−1489.
6. Nadra, A. D., Eliseo, T., Mok, Y. K., Almeida, C. L., Bycroft, M., Paci, M., de Prat-Gay, G., and Cicero, D. O. (2004) Solution structure of the HPV-16 E2 DNA binding domain, a transcriptional regulator with a dimeric β-barrel fold, *J. Biomol. NMR 30*, 211−214.
7. Liang, H., Petros, A. M., Meadows, R. P., Yoon, H. S. Y., Egan, D. A., Walter, K., Holzman, T. F., Robins, T., and Fesik, S. W. (1996) Solution structure of the DNA-binding domain of a human papillomavirus E2 protein: Evidence for flexible DNA-binding regions, *Biochemistry 35*, 2095−2103.
8. Hines, C. S., Meghoo, C., Shetty, S., Biburger, M., Brenowitz, M., and Hegde, R. S. (1998) DNA structure and flexibility in the sequence-specific binding of papillomavirus E2 proteins, *J. Mol. Biol. 276*, 809−818.

9. Hegde, R. S., Grossman, S. R., Laimins, L. A., and Sigler, P. B. (1992) The 1.7 Å crystal structure of the bovine papillomavirus-1 E2 DNA-binding domain bound to its DNA target, *Nature 359*, 505−512.
10. Kim, S. S., Tam, J. K., Wang, A. F., and Hegde, R. S. (2000) The structural basis of DNA target discrimination by papillomavirus E2 proteins, *J. Biol. Chem. 275*, 31245−31254.
11. Cicero, D. O., Nadra, A. D., Eliseo, T., Dellarole, M., Paci, M., and de Prat-Gay, G. (2006) Structural and thermodynamic basis for the enhanced transcriptional control by the human papillomavirus strain-16 E2 protein, *Biochemistry 45*, 6551−6560.
12. Lima, L. M., and Silva, J. L. (2004) Positive contribution of hydration on DNA binding by E2c protein from papillomavirus, *J. Biol. Chem. 279*, 47968−47974.
13. Brinda, K. V., Kannan, N., and Vishveshwara, S. (2002) Analysis of homodimeric protein interfaces by graph-spectral methods, *Protein Eng. 15*, 265−277.
14. Mok, Y.-K., Prat-Gay, G. D., Butler, P. J., and Bycroft, M. (1996) Equilibrium dissociation and unfolding of the dimeric human papillomavirus strain-16 E2 DNA-binding domain, *Protein Sci. 5*, 310−319.
15. Fesik, S. W. (1993) NMR structure-based drug design, *J. Biomol. NMR 3*, 261−269.
16. Pepinsky, R. B., Androphy, E. J., Corina, K., Brown, R., and Barsoum, J. (1994) Specific inhibition of a human papillomavirus E2 trans-activator by intracellular delivery of its repressor, *DNA Cell Biol. 13*, 1011−1019.
17. Kasukawa, H., Howley, P. M., and Benson, J. D. (1998) A fifteen-amino-acid peptide inhibits human papillomavirus E1−E2 interaction and human papillomavirus DNA replication in vitro, *J. Virol. 72*, 8166−8173.
18. Wang, Y., Coulombe, R., Cameron, D. R., Thauvette, L., Massariol, M. J., Amon, L. M., Fink, D., Titolo, S., Welchner, E., Yoakim, C., Archambault, J., and White, P. W. (2004) Crystal structure of the E2 transactivation domain of human papillomavirus type 11 bound to a protein interaction inhibitor, *J. Biol. Chem. 279*, 6976−6985.
19. Meisler, A. (2004) Characterization of the E2 protein from human papillomavirus strain 16 for study by NMR, M.Sc. Thesis, Tufts University, Boston, MA, pp 49−50.
20. Ferreiro, D. U., Dellarole, M., Nadra, A. D., and Prat-Gay, G. D. (2005) Free energy contribution to direct readout of a DNA sequence, *J. Biol. Chem. 280*, 32480−32484.
21. Edelhoch, H. (1967) Spectroscopic determination of tryptophan and tyrosine in proteins, *Biochemistry 6*, 1948−1954.
22. Pace, C. N., Shirley, B. A., and Thomson, J. A. (1989) Measuring the conformational stability of a protein, in *Protein Structure and Function, a Practical Approach* (Creighton, T., Ed.) pp 311−329, IRL Press, New York.
23. Royer, C. A., Mann, C. J., and Matthews, C. R. (1993) Resolution of the fluorescence equilibrium unfolding profile of Trp aporepressor using single tryptophan mutants, *Protein Sci. 2*, 1844−1852.
24. Thomson, J. A., Shirley, B. A., Grimsley, G. R., and Pace, C. N. (1989) Conformational stability and mechanism of folding of ribonuclease T1, *J. Biol. Chem. 264*, 11614−11620.
25. Bose, K., and Clark, A. C. (2001) Dimeric procaspase-3 unfolds via a four-state equilibrium process, *Biochemistry 40*, 14236−14242.
26. Bose, K., and Clark, A. C. (2005) pH effects on the stability and dimerization of procaspase-3, *Protein Sci. 14*, 24−36.
27. Veeraraghavan, S., Gilbert, G. D., and Baleja, J. D. (1998) Structure and topology of the membrane binding C2 domain of factor VIII in the presence of dodecylphosphocholine micelles, *Biochem. J. 332*, 549−555.
28. Primrose, W. U. (1992) Sample preparation, in *NMR of Macromolecules* (Roberts, G. C. K., Ed.) pp 22−23, Oxford University Press, Oxford, U.K.
29. Bradshaw, E. M., Sanford, D. G., Luo, X., Sudmeier, J., Gurard-Levin, Z. A., Bullock, P. A., and Bachovchin, W. W. (2004) T antigen origin-binding domain of simian virus 40: Determinants of specific DNA binding, *Biochemistry 43*, 6928−6936.
30. Lakowicz, J. R. (1999) General features of protein fluorescence, in *Principles of Fluorescence Spectroscopy*, pp 452−453, Plenum Press, New York.
31. Bhattacharyya, R., Saha, R. P., Samanta, U., and Chakrabarti, P. (2003) Geometry of interaction of the histidine ring with other planar and basic residues, *J. Proteome Res. 2*, 255−263.
32. Vito, C., Rodolfo, B., and Giuseppe, Z. (2003) High-resolution structures of retinol-binding protein in complex with retinol: pH-induced protein structural changes in the crystal state, *J. Mol. Biol. 329*, 841−850.
33. Bressanelli, S., Stiasny, K., Allison, S. L., Stura, E. A., Duquerroy, S., Lescar, J., Heinz, F. X., and Rey, F. A. (2004) Structure of a flavivirus envelope glycoprotein in its low-pH-induced membrane fusion conformation, *EMBO J. 28*, 723−733.
34. Blachon, S., Bellanger, S., Demeret, C., and Thierry, F. (2005) Nucleo-cytoplasmic shuttling of high risk human papillomavirus E2 proteins induces apoptosis, *J. Biol. Chem. 280*, 36088−36098.

BI0611255